Certifying the quantumness of a generalized coherent control scenario

Torsten Scholak[a)] and Paul Brumer
Chemical Physics Theory Group, Department of Chemistry, and Center for Quantum Information and Quantum Control, University of Toronto, Toronto, Ontario M5S 3H6, Canada

We consider the role of quantum mechanics in a specific coherent control scenario, designing a "coherent control interferometer" as the essential tool that links coherent control to quantum fundamentals. Building upon this allows us to rigorously display the genuinely quantum nature of a generalized weak-field coherent control scenario (utilizing 1 vs. 2 photon excitation) via a Bell-CHSH test. Specifically, we propose an implementation of "quantum delayed-choice" in a bichromatic alkali atom photoionization experiment. The experimenter can choose between two complementary situations, which are characterized by a random photoelectron spin polarization with particle-like behavior on the one hand, and by spin controllability and wave-like nature on the other. Because these two choices are conditioned coherently on states of the driving fields, it becomes physically unknowable, prior to measurement, whether there is control over the spin or not. © *2014 AIP Publishing LLC*. [http://dx.doi.org/10.1063/1.4902253]

I. INTRODUCTION

Various coherent control scenarios, in both complex and simple systems, utilize laser fields to coherently manipulate atomic or molecular fragmentation processes.[1] Two competing, fundamentally different perspectives have been advocated to explain the control. In the first, within the spirit of the Young double-slit experiment, one interprets the probability of the outcomes—the control target or yield—as an intensity and phase dependent pattern resulting from the quantum-coherent interference of mutually exclusive path alternatives that are embodied in the laser excitation pathways.[1–3] In the second, one views the controllability as the manifestation of the response of the system to the superposition of phase-coherent incident laser fields. In this approach, control is perceived as an inherently classical phenomenon,[4–6] i.e., a phenomenon that could fall under descriptions based on classical laws of motion. Understanding which of these descriptions is preferred is not just a matter of convenience. Rather, it has practical applications stemming from the recognition that decoherence effects often bring a system to the classical limit.[7] Hence, if control is indeed (at least partially) classical, then it may well survive in the often unavoidable decohering environments associated with realistic molecular processes.

There is ample motivation to address the issue of the role of quantum vs. classical effects in coherent control. For example, Refs. 8 and 9 analyze controlled symmetry breaking in a field-driven quartic oscillator both quantum-mechanically and classically and concludes that not only the basic requirements, but also the physical origins of control, are the same in both cases. Similarly, Ref. 10 shows that environmentally assisted one photon phase control is mainly due to the incoherent breaking of time-reversal symmetry, and is thereby not evidence of quantum coherent dynamics. In addition, it is of interest to note that related concerns regarding classical vs. quantum coherence contributions have arisen within the framework of electronic energy transfer in light-harvesting systems.[11]

Classical descriptions can offer an intuitively appealing picture, but in the case of coherent control they often fail quantitatively, and are hence discarded. Therefore, since its inception, coherent control has been regarded as fundamentally quantum,[1, 12, 13] particularly in the case of driving a system with two frequencies ($n\omega + m\omega$). Here, reliance on an interpretation of the interference of quantum pathways as described above (and as originally put forth[12, 13] by one of the authors of this paper) is commonly accepted. But the issue of the extent to which *nontrivial* quantum features are central to phenomena such as coherent control needs to be reconsidered in light of developments in Bell-like tests to certify unique quantum features[14–20] and recent reports that identify distinct classical mechanisms as a possible source of control.[5, 8–10, 21–23]

We reiterate that there is no question that quantum mechanics is necessary to *quantitatively* describe the outcome of coherent control scenarios. However, quantitative agreement with a quantum description cannot serve as a general proof that the observed phenomenon is unambiguously quantum in nature (since such a proof requires that all classical descriptions and explanations must be falsified). As a consequence, rigorously certifying the quantumness of a process and identifying its quantum features is a challenging task that has been the subject of intense efforts in quantum optics, quantum information, and quantum foundations. Studies of this type often take the form of proposed experimental protocols that are carefully crafted to close any loopholes that would prevent rigorous assertions regarding those features of quantum mechanics that are manifest in the process. Such features include issues such as nonlocality, entanglement, multiple-pathway interference, sensitivity to measurement, etc.[24] In

---
a)Electronic mail: tscholak@chem.utoronto.ca

this paper, we make the first inroads into utilizing ideas of this kind to explore the quantum characteristics of coherent control. Specifically, we first focus on path interference and introduce a "coherent control interferometer" (CCI) which formalizes the relationship between coherent control scenarios and quantum optics approaches to the fundamentals of quantum mechanics.[24,25] As a particular case, we concentrate the analysis on phase-coherent control over the spin polarization of an electron that has been emitted in an interfering ($\omega + 2\omega$) photoionization process.

We then design a *generalized* coherent control scenario in which measurements can be performed whose outcomes will have certifiably nonclassical statistics and that strongly support the analogy between coherent control and the quantum interference of paths. We show that this setup can be used to probe wave-particle complementarity and to implement "quantum delayed-choice";[18–20] it becomes unforeseeable prior to measurement whether the spin polarization statistics are wave- or particle-like, that is, whether there is control or not. This hallmark of quantum interference is key for violating a Bell inequality that serves as a rigorous experimental test of local realism and thereby distinguishes nonclassical from classical statistics, entirely on the basis of observed statistical data.[14–17]

Note the fact that we deal with a generalization of traditional coherent control scenarios indicates the continuing need to identify methods of certifying the quantumness of traditional coherent control scenarios. Such studies are underway and our expectation is that the coherent control interferometer introduced in this paper will serve as a central tool for such studies.

II. CONTROL SCENARIO

A. Coherent control interferometer

Let a heavy alkali atom be ionized by weak coherent ($\omega + 2\omega$) radiation.[26–28] For purposes of simplification (rather than physical necessity), we assume a tight confinement that fully suppresses decoherence due to recoil (c.f. Lamb-Dicke regime[64,65]),[29] The control target is the laboratory $\hat{z}$-axis projection m'_s of the photoelectron's spin in the continuum.[30,31] We consider the case where the continuum state $|K', m'_s{}^+\rangle$ of the electron at energy $E' = (\hbar K')^2/2m_e$ can be reached from the atomic ground state $|nS\frac{1}{2}, m_j\rangle$ mainly by two pathways:[32] (i) absorption of 1 photon of energy $\hbar\omega_2 = E' - E(nS\frac{1}{2})$ or (ii) of 2 photons each with energy $\hbar\omega_1 = \hbar\omega_2/2$. Here, K' refers to the electron's asymptotic outgoing wavevector,[32] n is the ground state's principle quantum number,[33] and the projection of the total angular momentum j onto the $\hat{z}$-axis is denoted m_j. This setup implements a CCI, Fig. 1, an analog of a Mach-Zehnder interferometer (MZI). The ground state is spin-$\frac{1}{2}$ and constitutes the CCI's two input ports whereas the final projections $m'_s = \pm\frac{1}{2}$ are identified with the two output ports, the measurement statistics $p_\pm$ of which are interpreted as the interference patterns. Henceforth, we restrict attention to one input port only, $m_j = -\frac{1}{2}$.

The incoming laser modes l are to be populated with coherent states of light, $|l\rangle \equiv |(\alpha k\hat{e})_l\rangle$, since these are eigen-
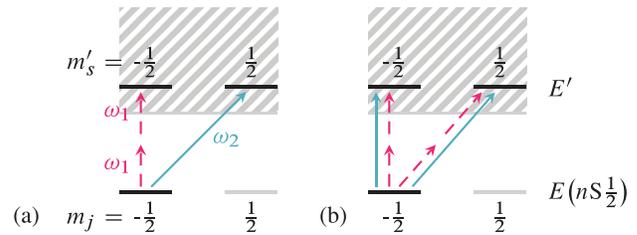

FIG. 1. Proposed coherent control interferometer (CCI). (a) In the open configuration o, single-photon ionization (solid blue) only undergoes a σ-transition with $|m_j - m'_s| = 1$, whereas two-photon ionization (dashed red) leaves the electron spin unchanged. The processes are distinguishable from one another due to their different outcomes. (b) This is not the case in the closed setup c, for which the transition amplitudes between all spin combinations are nonzero.

states of the photon annihilation operator and thus correlations with matter due to photon absorption do not occur.[34] The *a priori* probabilities of the ionization pathways can be adjusted by means of the amplitude moduli $|\alpha_l|$, the directions of incidence k_l, and the polarizations $\hat{\varepsilon}_l$. This is because (as described in Appendices A and B), in the long-time limit, the change of the electron's spin is described in terms of an infinite series of well-known, polarization-dependent transition matrix amplitudes $t_i(m'_s, m_j)$, $i = 1, 2, \ldots$, multiplied by corresponding powers of the field amplitudes α_l.[35–41] In the present case, only the first two transition amplitudes are relevant;[26,27] t_1 resolves the 1-photon process and connects only to P continuum states, whereas t_2 accounts for 2-photon ionization and accesses S and D orbitals. The amplitudes contain radial integrals, D_1 and D_2, that serve here as complex empirical parameters. There exist measurement schemes for which the ionization pathways become absolutely distinguishable. Therefore, in what follows, spin statistics are conditioned on successful detection of the electron in the channel $\hat{K}' = (\sqrt{2}\,\hat{x} - \hat{z})/\sqrt{3}$. This both eliminates the need for taking into account the efficiency of detection and does not provide information about the path taken from the initial to final state of the atom.

We argue that quantum interference in the CCI can be exposed in the same manner as it can be displayed in the Young double-slit,[42,43] a MZI, or a Ramsey interferometer[44,45] for single photons, electrons, etc. The latter undertaking entails the observation of complementarity between the wave and particle property, which is demonstrated by the experimenter's choice between two measurement statistics: particle and wave statistics. In the case of the former, interference is completely absent. In principle, if not in practice, knowledge about the path—whether the photon has taken the first rather than the second slit, or, correspondingly, whether the atom has been ionized in a 1- or a 2-photon process—is available by measurement. When it allows for tracing of paths, an interferometer is called open. If, in contrast, interference is displayed, then the statistics are wave-like. Full path knowledge cannot be acquired, not even in principle. This results from operating the interferometer in the so-called closed configuration. Below, the subscripts o and c are used to denote these configurations.

The ionization scenario has been selected because it is conducive to engineering both the o and c cases, Fig. 2.
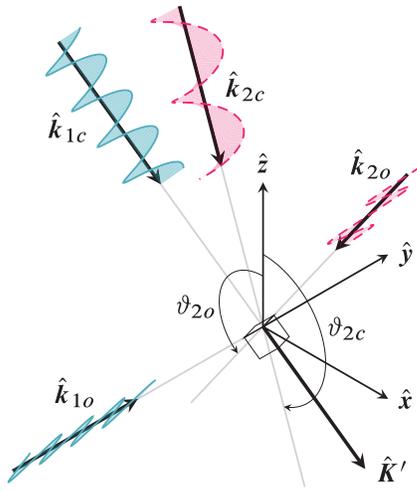
FIG. 2. Sample scattering geometry with incident light wavevectors $\hat{k}_{1o}$ = $\hat{y}$, $\hat{k}_{2o}$ with projection $\hat{k}_{2o} \cdot \hat{z} = \cos \vartheta_{2o} = -\sqrt{2/3}$, $\hat{k}_{1c} = \hat{K}'$, and $\hat{k}_{2c}$ with $\cos \vartheta_{2c} = -2\sqrt{2}/3$. The emitted photoelectron is detected in the direction $\hat{K}'$. The alkali atom is located at the origin. The polarization of the incoming radiation is indicated in color (shades of grey). The o configuration uses linear polarization, whereas the c setup employs elliptically polarized light.

1. The open interferometer configuration

For the open configuration, two linearly polarized modes, $(k\hat{e})_{1o}$ and $(k\hat{e})_{2o}$, are chosen, for example, to be populated according to $\hat{\boldsymbol{\varepsilon}}_{1o} = -\hat{k}_{2o} = (\hat{x} + \sqrt{2}\,\hat{z})/\sqrt{3}$ and $\hat{\boldsymbol{\varepsilon}}_{2o} = \hat{k}_{1o}$ = $\hat{y}$ in a field state denoted $|1o, 2o\rangle$. The vectors $\hat{K}'$, $\hat{k}_{2o}$, and $\hat{k}_{1o}$ come as a right-handed orthogonal triad that is inclined at an angle $\pi - \arctan(\sqrt{2})$ away from the positive $\hat{z}$-axis. These mode settings imply $t_{1o} \propto \delta_{m'_s, -m_j}$ and $t_{2o} \propto \delta_{m'_s, m_j}$ and, as a result, absolute path knowledge; the direction in which the spin is detected reveals the path taken through the CCI, cf. Figs. 1(a) and 2. To realize an unbiased interferometer, the moduli of the complex amplitudes are to be adjusted as follows:

$$|\alpha_{1o}| = \frac{6\sqrt{\pi}\,\lambda e^{i\kappa_{1o}}}{\hbar g_{k_1}\left[-D_1\left(E'P\frac{1}{2}, nS\frac{1}{2}\right) + D_1\left(E'P\frac{3}{2}, nS\frac{1}{2}\right)\right]}, \quad (1a)$$

$$|\alpha_{2o}|^2 = \frac{90\sqrt{\pi}\,\lambda e^{i\kappa_{2o}}}{i\hbar^2 g_{k_2}^2}\Big[-5D_2\left(E'S\frac{1}{2}, P\frac{1}{2}, nS\frac{1}{2}\right)$$

$$- 10D_2\left(E'S\frac{1}{2}, P\frac{3}{2}, nS\frac{1}{2}\right) + 5D_2\left(E'D\frac{3}{2}, P\frac{1}{2}, nS\frac{1}{2}\right)$$

$$+ D_2\left(E'D\frac{3}{2}, P\frac{3}{2}, nS\frac{1}{2}\right) + 9D_2\left(E'D\frac{5}{2}, P\frac{3}{2}, nS\frac{1}{2}\right)\Big]^{-1}. \quad (1b)$$

Equations (1) define conditions on the phases κ_{1o} and κ_{2o} that ensure that the right hand sides of Eqs. (1a) and (1b) are real and nonnegative. κ_{1o} and κ_{2o} therefore depend on the complex phases of the integrals D_1 and D_2 and will henceforth be referred to as material phases. The arguments of D_1 and D_2 refer to the respective photoionization channels. For example, $D_2(E'D\frac{5}{2}, P\frac{3}{2}, nS\frac{1}{2})$ is the radial matrix element of the pro-

cess leading from the ground state $|nS\frac{1}{2}, m_j\rangle$ via intermediate $P\frac{3}{2}$ orbitals to the continuum state $|E'D\frac{5}{2}, m_j'^{+}\rangle$. The field's phases, $\phi_{1o} = \text{Arg}\,\alpha_{1o}$ and $\phi_{2o} = \text{Arg}\,\alpha_{2o}$, can still be chosen freely. In Eqs. (1), λ is a positive, constant scaling factor. The precise value of λ is irrelevant, since the probability amplitudes are eventually conditioned on successful detection of the photoelectron in the channel $\hat{K}'$. For the choices above, $|t_{1o}\alpha_{1o}| = |t_{2o}\alpha_{2o}^2|$. We have thus established that, for the initial state $|nS\frac{1}{2}, -\frac{1}{2}\rangle \otimes |1o, 2o\rangle$, the final state of the ionized atom in the channel $\boldsymbol{K}'$ is $|f_o\rangle \otimes |1o, 2o\rangle$, where

$$|f_o\rangle = \frac{e^{i\delta_o}}{\sqrt{2}}\left(|\boldsymbol{K}', \tfrac{1}{2}^{+}\rangle + e^{-i\theta_o}|\boldsymbol{K}', -\tfrac{1}{2}^{+}\rangle\right) \quad (2)$$

with $\delta_o = \phi_{1o} + \kappa_{1o}$ and $\theta_o = \phi_{1o} - 2\phi_{2o} + \kappa_{1o} - \kappa_{2o}$. The state $|f_o\rangle$ describes full particle-like statistics; projected onto the $\hat{z}$ axis, both spin orientations $m'_s = \pm\frac{1}{2}$ are always equally likely, regardless of the lasers' phase difference $\phi_{1o} - 2\phi_{2o}$. Thus, there is no phase-coherent control and the fringe visibility vanishes on both output ports.

2. The closed interferometer configuration

As for the closed configuration c, it can be achieved by populating two other modes, $(k\hat{e})_{1c}$ and $(k\hat{e})_{2c}$ (see Fig. 2). For example, the one-photon absorption field $1c$ is chosen circularly polarized, $\sqrt{14}\,\hat{\boldsymbol{e}}_{1c} = \sqrt{5/3 + \sqrt{2}}(\hat{x} + \sqrt{2}\,\hat{z})$ $- i\sqrt{9 - 3\sqrt{2}}\,\hat{y}$ with $\hat{k}_{1c} = \hat{K}'$, whereas the two-photon absorption field $2c$ is chosen elliptically polarized, $\sqrt{2}\,\hat{\boldsymbol{e}}_{2c} = (2\sqrt{2}\,\hat{x} + \hat{z})/3 + i\hat{y}$ as well as $\hat{k}_{2c} = (\hat{x} - 2\sqrt{2}\,\hat{z})/3$, making an angle of $\pi - \text{arccsc}(3)$ with the $\hat{z}$-axis. The resultant field state is denoted $|1c, 2c\rangle$. Only $t_2(\frac{1}{2}, \frac{1}{2})$ and $t_2(-\frac{1}{2}, -\frac{1}{2})$ contain S-wave D_2 factors. They are fully suppressed in the chosen field configuration. (It turns out that simultaneous unbiased interference for both input ports of the CCI, $m_j = \pm\frac{1}{2}$, cannot be achieved. That is why the above settings are tailored specifically to balance the interference from the input port $m_j = -\frac{1}{2}$.) With these, we find $t_{1c}(\frac{1}{2}, -\frac{1}{2})$ $= t_{1c}(-\frac{1}{2}, -\frac{1}{2})$. Although it would be most desirable to also have $t_{2c}(\frac{1}{2}, -\frac{1}{2}) = -t_{2c}(-\frac{1}{2}, -\frac{1}{2})$, the latter amplitudes are somewhat biased and have generally a mutual phase shift different from π. This is the case unless one can select an energy E' for which the transition to $j' = \frac{5}{2}$ is negligible compared to $j' = \frac{3}{2}$; indeed, for $D_2(E'D\frac{5}{2}, P\frac{3}{2}, nS\frac{1}{2}) = 0$, the t_{2c} are as desired. If this were the case the amplitudes would be set equal in absolute value to

$$|\alpha_{1c}| = \sqrt{\tfrac{7}{2(3-\sqrt{2})}}\,|\alpha_{1o}|, \quad (3a)$$

$$|\alpha_{2c}|^2 = \frac{180\sqrt{\pi}\,\lambda e^{i\kappa_{2c}}}{i(\sqrt{2}+2)\hbar^2 g_{k_2}^2}\Big[5D_2\left(E'D\frac{3}{2}, P\frac{1}{2}, nS\frac{1}{2}\right)$$

$$+ D_2\left(E'D\frac{3}{2}, P\frac{3}{2}, nS\frac{1}{2}\right)\Big]^{-1}, \quad (3b)$$

in order to achieve unbiased interference. We choose the amplitudes (3) even for cases where $D_2(E'D\frac{5}{2}, P\frac{3}{2}, nS\frac{1}{2}) \neq 0$. The phases $\phi_{1c} = \text{Arg}\,\alpha_{1c}$ and $\phi_{2c} = \text{Arg}\,\alpha_{2c}$ are free parameters, whereas κ_{2c} is another constant material phase that is implicitly defined by Eq. (3b). The phases picked up by the

one-photon processes are identical in the configurations o and c, therefore $\kappa_{1c} = \kappa_{1o}$. Consider now initialization from the state $|nS\frac{1}{2}, -\frac{1}{2}\rangle \otimes |1c, 2c\rangle$. For successful detection in the channel $\boldsymbol{K}'$, the final state becomes $|f_c\rangle \otimes |1c, 2c\rangle$, where

$$|f_c\rangle = \frac{e^{i\delta_c}}{N_{f_c}} \left[\left(i \sin\frac{\phi_c + \theta_c}{2} - e^{-i\phi_c/2} d_2 \right) \left| \boldsymbol{K}', \frac{1}{2}^+ \right\rangle \right.$$
$$\left. + \left(\cos\frac{\phi_c + \theta_c}{2} + \left(\frac{7}{2} - \frac{5}{\sqrt{2}}\right) e^{-i\phi_c/2} d_2 \right) \left| \boldsymbol{K}', -\frac{1}{2}^+ \right\rangle \right]$$

(4)

with the global phase $\delta_c = (\phi_{1c} + 2\phi_{2c} + \kappa_{1c} + \kappa_{2c})/2$, the interferometric phase difference $\phi_c = \phi_{1c} - 2\phi_{2c}$, the material phase shift $\theta_c = \kappa_{1c} - \kappa_{2c}$, the normalization N_{f_c}, and with

$$d_2 = \frac{-3i \, e^{-i(\kappa_{1c} + \kappa_{2c})/2} D_2 \left(E' D\frac{5}{2}, P\frac{3}{2}, nS\frac{1}{2} \right)}{\left| 5 D_2 \left(E' D\frac{3}{2}, P\frac{1}{2}, nS\frac{1}{2} \right) + D_2 \left(E' D\frac{3}{2}, P\frac{3}{2}, nS\frac{1}{2} \right) \right|}. \quad (5)$$

The state $|f_c\rangle$ is wave-like; coherent control of the electron's spin is possible by virtue of the phase ϕ_c. The interference contrast is maximal for $D_2(E'D\frac{5}{2}, P\frac{3}{2}, nS\frac{1}{2}) = 0$, in which case also $d_2 = 0$ and $|t_{1c}(m_s', -\frac{1}{2})\alpha_{1c}| = |t_{2c}(m_s', -\frac{1}{2})\alpha_{2c}^2|$.

B. Complementarity

Complementarity in quantum interference demands that the experimental situation determines whether one detects the statistics of a wave or a particle (or even a blend of the two).[46,47] In classical physics, these concepts are mutually exclusive, and the object passing the interferometer cannot subscribe to either of them *ad libitum*. In order to stress this fundamental difference, Wheeler proposed the "delayed-choice" experiment[48] that severs any causal link between the object and the interferometer until it has entered it. If we wanted to realize Wheeler's[48] gedanken experiment with coherent control, we would have to postpone and randomize the choice between o and c such that the spin cannot "know" beforehand which property to display. The proposed CCI does not, however, literally allow this, because randomization between $|1o, 2o\rangle$ and $|1c, 2c\rangle$ would choose the "control" or "no control" in advance. (Indeed, this is the central stumbling block to considering features of complementarity in coherent control scenarios.) Notwithstanding, instead of flipping a coin between o and c, we can design a generalized coherent control scenario where one prepares a coherent superposition $|i\rangle = |nS\frac{1}{2}, -\frac{1}{2}\rangle \otimes (|1o, 2o\rangle + |1c, 2c\rangle)/N_i$ that gives the final state

$$|f\rangle = \frac{1}{N_f} \left(|f_o\rangle \otimes |1o, 2o\rangle + N_{f_c} |f_c\rangle \otimes |1c, 2c\rangle \right) \quad (6)$$

with N_i, N_f being normalization factors. Since the states $|1o, 2o\rangle$ and $|1c, 2c\rangle$ are each direct products of two coherent states in, in total, four mutually orthogonal modes, the initial state $|i\rangle$ features nonclassical correlations of the GHZ type[17,49–51] the creation of which requires a special nonlinear MZI.[52] By contrast, the resultant final state $|f\rangle$ of the total system describes entanglement between the radiation field and the electron spin. It is a coherent blend of particle- and wave-like spin

polarization statistics that is conditioned on the state of the radiation field. As such, the field-matter entanglement plus the superposition state character of Eq. (6) allows for the delayed-choice determination of whether the system is in $|f_o\rangle$ or $|f_c\rangle$ conditioned on the measurement of the field.

C. Bell test

We still owe a test that can certify the nonclassicality of an actual experimental realization of the CCI. Such test is mandatory, since only if the correlations between the radiation field and the electron spin are of nonclassical nature, we can truly delay the choice of whether the spin statistics are that of a particle or a wave. The statistics must be unknowable prior to the measurement of the field. A test for nonclassicality is provided by a certain family of Bell-CHSH inequalities that are derived from the concept of local realism.[14–17] Adapting the approach of Ref. 53, we define two parametric dichotomic measurement operators: The operator $\Gamma(\zeta) = R(\zeta)^\dagger \sigma_z R(\zeta)$ with the rotation $R(\zeta) = \exp(\zeta \sigma_+ - \zeta^* \sigma_-)$ measures the spin asymmetry in the direction of space defined by the complex number ζ. Here, the Pauli operators σ_z, $\sigma_\pm$ are defined with respect to the basis $\{|\boldsymbol{K}', \frac{1}{2}^+\rangle, |\boldsymbol{K}', -\frac{1}{2}^+\rangle\}$. The observable $A(\boldsymbol{\beta}) = \bigotimes_l F_l(\beta_l)^\dagger \cdot (2|\text{vac}\rangle\langle\text{vac}| - 1) \cdot \bigotimes_{l'} F_{l'}(\beta_{l'})$ with the displacements $F_l(\beta_l) = \exp(\beta_l a_l^\dagger - \beta_l^* a_l)$ allows for a joint photon threshold measurement over all modes $l = 1o, 1c, 2o,$ and $2c$, where $|\text{vac}\rangle$ denotes the vacuum state, in all modes, of the radiation field.

As described in Appendix D, we have calculated numerically the maximally achievable violation of the Bell-CHSH inequality

$$|\langle B \rangle| \equiv |\langle \Gamma(\zeta) \otimes A(\boldsymbol{\beta}) \rangle + \langle \Gamma(\zeta') \otimes A(\boldsymbol{\beta}) \rangle$$
$$+ \langle \Gamma(\zeta) \otimes A(\boldsymbol{\beta}') \rangle - \langle \Gamma(\zeta') \otimes A(\boldsymbol{\beta}') \rangle| \le 2 \quad (7)$$

by measurements on a system in the state $|f\rangle$ as a function of ϕ for different photon detection efficiencies η. The primed parameters ζ', $\boldsymbol{\beta}'$ define an additional set of observables. To incorporate limited efficiency, each mode is attenuated by a beam splitter with transmissivity $\sqrt{\eta}$ before ideal detection.[53,54] The statistical error in the photoelectron polarization asymmetry measurements is not addressed at this time.[55] Significantly, as is evident from Fig. 3, Bell's inequality can be violated to various degrees for all phases ϕ, where $\phi = -\phi_c - \theta_c = \pi/2 - \theta_o$, if $\eta > 0.5$. For $\phi = 0$ and $\eta = 1$, $|\langle B \rangle|$ can even reach the Tsirelson bound $2\sqrt{2}$, the maximum allowed by quantum mechanics.[56,57] For every ϕ, the maximum violation is independent of the absolute field amplitudes $|\alpha_l|$, since the parameters $|\beta_l|$ and $|\beta_l'|$ can always be adapted accordingly. The optimized complex phases of the $\boldsymbol{\beta}$ and $\boldsymbol{\beta}'$ vary piecewise continuously with ϕ,[58] and they are independent of $|\alpha_l|$. So too are the optimal choices for ζ and ζ'. Additional numerical experiments have shown that successful Bell test violation does not critically depend on how small d_2 is; near to maximum violations can still be achieved if $|d_2|$ is of the order of 1, see Appendix D.

We can now summarize as follows: The coherent control interferometer configurations, o and c, create experimental conditions under which a particle and a wave property,
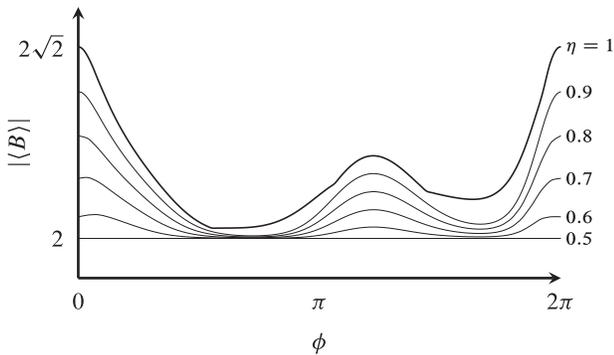
FIG. 3. Numerically optimized Bell-CHSH inequality test for $|f\rangle$ as a function of the phase ϕ. The Bell inequality can be violated as long as the detection efficiency η is larger than 0.5. For ideal photodetectors ($\eta = 1$), the violation can be saturated, $|\langle B \rangle| = 2\sqrt{2}$ at $\phi = 0$; the smallest violation is 2.044. Here, for simplicity, $\phi = -\phi_c - \theta_c = \pi/2 - \theta_o$.

respectively, are displayed. In the specific scenario that starts with the initial state $|i\rangle$ (above Eq. (6)), the coherent control dynamics transform the initial GHZ entanglement between the modes of the field into all-encompassing nonclassical EPR correlations between spin and radiation. If a Bell violation is found (for a range of different ϕ), then it is unknowable whether the measured spin statistics are that of a wave or a particle and thus whether control is possible or not. The outcome is physically guaranteed to be random and the experiment implements "quantum delayed-choice."[18–20,59–62]

III. DISCUSSION

It is advantageous to make explicit the difference between the traditional understanding of the quantum character of coherent control and the view considered in this paper. It is commonly agreed that, in the perturbative limit, the properties of the driving fields and of the atomic or molecular system independently contribute to the response.[1,6] In multi-color laser-induced coherent control, for example, control via phase sensitivity emerges solely from cross terms containing products of the $n\omega$ and $m\omega$ driving field amplitudes. This basic mechanism is common to all classical and quantum descriptions of weak-field ($n\omega + m\omega$) coherent control.[1,8,23] It has led research to be primarily concerned with the *magnitude* of the terms giving rise to phase dependence and, in view of quantum-classical correspondence, whether this magnitude depends crucially on quantum effects such as tunneling[6] or conservation of parity.[8] In other words, the divide between quantum and classical control has been defined in terms of quantitative indicators only, indicators which require a comparison of classical and quantum model calculations as a means of assessing the importance of quantum features.

By contrast, we focus here on a fundamentally qualitative feature: the non-local character of the proposed light-matter scenario. The resultant physics in the generalized coherent control scenario described here rules out any local realistic (classical) theory, because controllability is conditioned on nonclassical correlations between matter and radiation. In the experiment, this is ascertainable *a posteriori* by virtue of a Bell-CHSH test. Introducing such a test has required, how-

ever, that we go beyond traditional coherent control scenarios to introduce and examine a generalized scenario allowing a Bell-CHSH test. Studies refocusing attention on traditional coherent control scenarios are underway.

APPENDIX A: SCATTERING MATRIX

We examine here the interaction between a single heavy alkali atom and ionizing bichromatic radiation. As explained in the main text atomic motion is not considered, because the atom is assumed to be tightly trapped. Neglecting hyperfine structure, we specify the hydrogen-like electronic bound states in the standard spectroscopic notation as $|nlj, m_j\rangle$ with n the principle quantum number and $E(nlj)$ the energy. The continuum states are denoted either by $|Elj, m_j{}^+\rangle$ with l the orbital and j the total angular momentum or by $|\boldsymbol{K}, m_s{}^+\rangle$, where $\boldsymbol{K}$ refers to the electron's asymptotic outgoing wavevector.[32] In the basis of bound and continuum states, the atomic Hamiltonian H_A is diagonal. The bound and continuum solutions R_{nlj}, R_{Elj} of the radial Schrödinger equation depend on both the orbital angular momentum l and the total angular momentum j; m_j denotes its projection onto the $\hat{\boldsymbol{z}}$-axis in the laboratory frame. Using Clebsch-Gordan coefficients, we write

$$\langle \boldsymbol{x}|nlj, m_j \rangle = \sum_{m_l m_s} \langle lm_l, \tfrac{1}{2}m_s | jm_j \rangle R_{nlj}(x) Y_{lm_l}(\hat{\boldsymbol{x}}) |m_s\rangle,$$

(A1)

where m_l is the orbital angular momentum's projection on the $\hat{\boldsymbol{z}}$-axis and $|m_s\rangle$ describes the electron's spin projected onto the same axis. An analogous expansion exists for the continuum wave functions $\langle \boldsymbol{x}|Elj, m_j{}^+\rangle$. The quantized radiation field, with canonical Hamiltonian $H_{\mathcal{R}}$, constitutes an auxiliary degree of freedom $\mathcal{R}$. We treat the light-matter interaction V within the electric dipole approximation,

$$V = e \sum_{\boldsymbol{k}\hat{\boldsymbol{\varepsilon}}} \hbar g_k (\mathrm{i}\, a_{\boldsymbol{k}\hat{\boldsymbol{\varepsilon}}}\, \boldsymbol{x} \cdot \hat{\boldsymbol{\varepsilon}} + \text{h.c.}),$$

(A2)

where g_k is the vacuum field strength and $a_{\boldsymbol{k}\hat{\boldsymbol{\varepsilon}}}$ the photon annihilation operator with wave vector $\boldsymbol{k} = \omega_k \hat{\boldsymbol{k}}/c$ and polarization $\hat{\boldsymbol{\varepsilon}} \perp \boldsymbol{k}$. In the long-time limit, the change of the electron's spin can be described by a completely positive map that is constructed from matrix elements

$$\langle \boldsymbol{K}', m_s'{}^+; m'\boldsymbol{k}\hat{\boldsymbol{\varepsilon}}|S|n\mathrm{S}\tfrac{1}{2}, m_j; m\boldsymbol{k}\hat{\boldsymbol{\varepsilon}}\rangle$$

(A3)

of the scattering operator

$$S = 1 - 2\pi \mathrm{i} \int \mathrm{d}E \delta(E - H_0) T(E + \mathrm{i}0)\delta(E - H_0),$$ (A4)

where $|m\boldsymbol{k}\hat{\boldsymbol{\varepsilon}}\rangle$ is the m-photon number state of the mode $\boldsymbol{k}\hat{\boldsymbol{\varepsilon}}$ and $H_0 = H_A + H_{\mathcal{R}}$ the free Hamiltonian of atom and

radiation. The transition operator T has a perturbative expansion $T(z) = V + V G_0(z) T(z)$ in powers of V and the unperturbed resolvent $G_0(z) = (z - H_0)^{-1}$.

APPENDIX B: TRANSITION AMPLITUDES

The relevant transition amplitudes are well known[26,27] and can be written in terms of first and second order angular, A_1, A_2, and radial, D_1, D_2, dipole matrix elements. For completeness, we present their straightforward derivation.

Evaluating the scattering matrix element, Eq. (A3), to first order gives the probability amplitude for the absorption of a single photon and ejecting an electron with asymptotic wavevector $\boldsymbol{K}'$: $\frac{1}{\hbar}\delta(\omega - \omega_1) \delta_{m,m'+1} \sqrt{m}\, t_1(m'_s, m_j)$ with $\omega = ck$ and

$$
t_1(m'_s, m_j) = \frac{2\pi\hbar^2 g_k}{\sqrt{m_e K'}} \sum_{m'_l} Y_{1m'_l}(\hat{\boldsymbol{K}}') \sum_{j'm'_j} \left\langle 1m'_l, \tfrac{1}{2}m'_s \middle| j'm'_j \right\rangle
$$
$$
\times \left\langle m'_j \middle| A_1\left(\mathrm{P}j', \mathrm{S}\tfrac{1}{2};\hat{\epsilon}\right) \middle| m_j \right\rangle D_1\left(E'\mathrm{P}j', n\mathrm{S}\tfrac{1}{2}\right). \tag{B1}
$$

The dipole selection rules dictate that t_1 only connects to P continuum states, $l' = 1$ (see also Fig. 4). This finds expression in the angular dipole matrix element,

$$
\left\langle m'_j \middle| A_1\left(l'j', lj;\hat{\boldsymbol{\epsilon}}\right) \middle| m_j \right\rangle
$$
$$
= \sqrt{\frac{2l+1}{2l'+1}} \langle l0, 10|l'0\rangle \sum_{m_l m'_l} \sum_q \varepsilon_q \langle lm_l, 1q|l'm'_l\rangle
$$
$$
\times \sum_{m_s} \left\langle l'm'_l, \tfrac{1}{2}m_s \middle| j'm'_j \right\rangle \left\langle lm_l, \tfrac{1}{2}m_s \middle| jm_j \right\rangle, \tag{B2}
$$

which vanishes unless l and l' differ by one. Moreover, the projections $\varepsilon_q = \hat{\boldsymbol{\epsilon}} \cdot \hat{\boldsymbol{e}}_q^*$ of the incident-field polarization onto the spherical basis vectors $\hat{\boldsymbol{e}}_{\pm 1} = \mp(\hat{\boldsymbol{x}} \pm \hat{\boldsymbol{y}})/\sqrt{2}$, $\hat{\boldsymbol{e}}_0 = \hat{\boldsymbol{z}}$ determine the respective shares of σ-($\Delta m_j = \pm 1$) and π-transitions ($\Delta m_j = 0$) in the absorption amplitude. The radial integrals,[36,37] $D_1(E'l'j', nlj) = e\int_0^\infty \mathrm{d}x\, x^3 R^*_{E'l'j'}(x) R_{nlj}(x)$, etc., shall not be explicitly calculated here and serve as empirical parameters. In the same manner, we derive the two-photon transition amplitude in second order perturbation theory. It can be written as
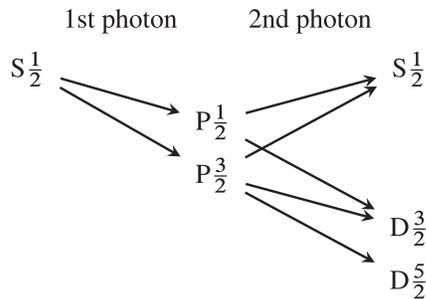

FIG. 4. Electric dipole selection rules between lj-states in one- and two-photon absorption. These two processes are distinguishable by the final orbital angular momenta, in particular, the separation into states with even (S, D) and those with odd parity (P).

$\frac{1}{2\hbar}\delta(\omega - \omega_2)\delta_{m,m'+2}\sqrt{m(m-1)}\, t_2(m'_s, m_j)$, where we defined

$$
t_2(m'_s, m_j)
$$
$$
= \frac{2\pi\mathrm{i}\hbar^3 g_k^2}{\sqrt{m_e K'}} \sum_{l'm'_l} Y_{l'm'_l}(\hat{\boldsymbol{K}}') \sum_{j'm'_j} \left\langle l'm'_l, \tfrac{1}{2}m'_s \middle| j'm'_j \right\rangle
$$
$$
\times \sum_{j''} \left\langle m'_j \middle| A_2\left(l'j', \mathrm{P}j'', \mathrm{S}\tfrac{1}{2};\hat{\epsilon}\right) \middle| m_j \right\rangle D_2\left(E'l'j', \mathrm{P}j'', n\mathrm{S}\tfrac{1}{2}\right), \tag{B3}
$$

$$
\left\langle m'_j \middle| A_2(l'j', l''j'', lj;\hat{\epsilon}) \middle| m_j \right\rangle
$$
$$
= \sum_{m''_j} \left\langle m'_j \middle| A_1\left(l'j', l''j'';\hat{\epsilon}\right) \middle| m''_j \right\rangle \left\langle m''_j \middle| A_1\left(l''j'', lj;\hat{\epsilon}\right) \middle| m_j \right\rangle, \tag{B4}
$$

and

$$
D_2\left(E'l'j', l''j'', nlj\right)
$$
$$
= \sum_{n''} \frac{D_1\left(E'l'j', n''l''j''\right) D_1\left(n''l''j'', nlj\right)}{E' - E\left(n''l''j''\right) - \hbar ck + \mathrm{i}0}
$$
$$
+ \int \mathrm{d}E'' \frac{D_1\left(E'l'j', E''l''j''\right) D_1\left(E''l''j'', nlj\right)}{E' - E'' - \hbar ck + \mathrm{i}0}. \tag{B5}
$$

Inspection of the selection rules reveals that, for the two-photon process, only partial waves with $l' = 0$ or 2 contribute to the final amplitude, cf. Fig. 4.

APPENDIX C: FINITE DETECTION EFFICIENCY

It can be expected that an inefficient measurement of the electron spin polarization affects the Bell inequality violation in a qualitatively similar manner as an inefficient photon threshold measurement. We therefore concern ourselves only with the latter. A photodetector with limited photodetection efficiency can be modelled as an ideal photodetector behind an output port of an unbiased beam splitter. Let that beam splitter have the transmissivity $\sqrt{\eta}$. The photodetection with efficiency η is adequately described if we calculate the expectation value of the CHSH-Bell operator B with respect to the state

$$
|f'\rangle = B_{1o}(\eta) B_{2o}(\eta) B_{1c}(\eta) B_{2c}(\eta) |f\rangle, \tag{C1}
$$

where the beam splitter operator B_{1o} couples the mode $1o$ to the auxiliary mode $1o'$,

$$
B_{1o}(\eta) = \exp\left[\arccos\sqrt{\eta}\left(a_{1o}^\dagger a_{1o'} - a_{1o} a_{1o'}^\dagger\right)\right]. \tag{C2}
$$

The operators B_{2o}, B_{1c}, and B_{2c} are defined analogously.

APPENDIX D: NUMERICAL OPTIMIZATION OF $|\langle B\rangle|$

The Bell-CHSH observable B depends on a variety of measurement settings. For a range of final states $|f'\rangle$, parametrized by the phase ϕ (and the detection efficiency η), we want to find the settings for B that allow for the maximum violation of the Bell-CHSH inequality (7).

Introducing the phase ϕ (see the main text) is equivalent to phase-locking the complex amplitudes α_{1o}, α_{2o}, α_{1c}, and α_{2c} in the following way:

$$\text{Arg}\,\alpha_{1o} \equiv \phi_{1o} = -\frac{\pi}{2} - \kappa_1 + \kappa_{2o} + 2\phi_{2c}, \qquad \text{(D1a)}$$

$$\text{Arg}\,\alpha_{2o} \equiv \phi_{2o} = \frac{1}{2}(-\pi - \kappa_{2o} + \kappa_{2c} + \phi + 2\phi_{2c}), \quad \text{(D1b)}$$

$$\text{Arg}\,\alpha_{1c} \equiv \phi_{1c} = -\kappa_1 + \kappa_{2c} - \phi + 2\phi_{2c}. \qquad \text{(D1c)}$$

Here, we are free to set $\phi_{2c} \equiv \text{Arg}\,\alpha_{2c} = 0$, since the expectation value of the Bell-CHSH observable does not depend on this particular phase.

For now, let us also assume that $d_2 = 0$. We then have $N_{f_c} = 1$ and

$$
\begin{aligned}
\langle f'|\Gamma\,(\zeta)\otimes A\,(\boldsymbol{\beta})|f'\rangle = N_f^{-2}(&\langle f_o|\Gamma\,(\zeta)|f_o\rangle\langle\sqrt{\eta}\alpha_{1o}, \sqrt{\eta}\alpha_{2o}, 0, 0|A\,(\boldsymbol{\beta})|\sqrt{\eta}\alpha_{1o}, \sqrt{\eta}\alpha_{2o}, 0, 0\rangle \\
&+ \langle f_o|\Gamma\,(\zeta)|f_c\rangle\langle\sqrt{\eta}\alpha_{1o}, \sqrt{\eta}\alpha_{2o}, 0, 0|A\,(\boldsymbol{\beta})|0, 0, \sqrt{\eta}\alpha_{1c}, \sqrt{\eta}\alpha_{2c}\rangle e^{-(1-\eta)\|\boldsymbol{\alpha}\|^2/2} \\
&+ \langle f_c|\Gamma\,(\zeta)|f_o\rangle\langle 0, 0, \sqrt{\eta}\alpha_{1c}, \sqrt{\eta}\alpha_{2c}|A\,(\boldsymbol{\beta})|\sqrt{\eta}\alpha_{1o}, \sqrt{\eta}\alpha_{2o}, 0, 0\rangle e^{-(1-\eta)\|\boldsymbol{\alpha}\|^2/2} \\
&+ \langle f_c|\Gamma\,(\zeta)|f_c\rangle\langle 0, 0, \sqrt{\eta}\alpha_{1c}, \sqrt{\eta}\alpha_{2c}|A\,(\boldsymbol{\beta})|0, 0, \sqrt{\eta}\alpha_{1c}, \sqrt{\eta}\alpha_{2c}\rangle)
\end{aligned}
\qquad \text{(D2)}
$$

with $N_f^2 = 2 + \frac{1}{\sqrt{2}}\left[\sin\phi - \cos\phi - \cos(2\phi)\right]e^{-\|\boldsymbol{\alpha}\|^2/2}$,

$$\langle f_o|\Gamma\,(\zeta)|f_o\rangle = -\sin(2|\zeta|)\sin(\phi + \text{Arg}\,\zeta), \qquad \text{(D3a)}$$

$$
\begin{aligned}
\langle f_o|\Gamma\,(\zeta)|f_c\rangle = \frac{1}{\sqrt{2}}\exp\left[-\mathrm{i}\left(\frac{\pi}{4} + \phi\right)\right]&\left[\cos(2|\zeta|)\left(\frac{\mathrm{i}}{\sqrt{2}} + \sin\left(\frac{\pi}{4} + \phi\right)\right)\right. \\
&\left.+ \sin(2|\zeta|)\left(-\mathrm{i}\sin\left(\frac{\pi}{4} + \phi\right) + \sin\left(\frac{\pi}{4} + \phi + \text{Arg}\,\zeta\right)\right)\right],
\end{aligned}
\qquad \text{(D3b)}
$$

$$
\begin{aligned}
\langle f_c|\Gamma\,(\zeta)|f_o\rangle = \frac{1}{\sqrt{2}}\exp\left[\mathrm{i}\left(\frac{\pi}{4} + \phi\right)\right]&\left[\cos(2|\zeta|)\left(-\frac{\mathrm{i}}{\sqrt{2}} + \sin\left(\frac{\pi}{4} + \phi\right)\right)\right. \\
&\left.+ \sin(2|\zeta|)\left(\mathrm{i}\sin\left(\frac{\pi}{4} + \phi\right) + \sin\left(\frac{\pi}{4} + \phi + \text{Arg}\,\zeta\right)\right)\right],
\end{aligned}
\qquad \text{(D3c)}
$$

$$\langle f_c|\Gamma\,(\zeta)|f_c\rangle = -\cos(2|\zeta|)\cos\phi + \sin(2|\zeta|)\sin(\text{Arg}\,\zeta)\sin\phi, \qquad \text{(D3d)}$$

and

$$\langle\boldsymbol{\alpha}|A\,(\boldsymbol{\beta})|\boldsymbol{\alpha}'\rangle = e^{-(\|\boldsymbol{\alpha}\|^2 + \|\boldsymbol{\alpha}'\|^2)/2}(2e^{-\|\boldsymbol{\beta}\|^2 - \boldsymbol{\alpha}^*\cdot\boldsymbol{\beta} - \boldsymbol{\alpha}'\cdot\boldsymbol{\beta}^*} - e^{\boldsymbol{\alpha}^*\cdot\boldsymbol{\alpha}'}). \qquad \text{(D3e)}$$

From these expressions it becomes clear that the Bell-CHSH expectation value $\langle f'|B|f'\rangle = \langle f'|\Gamma(\zeta)\otimes A(\boldsymbol{\beta})|f'\rangle + \langle f'|\Gamma(\zeta')\otimes A(\boldsymbol{\beta})|f'\rangle + \langle f'|\Gamma(\zeta)\otimes A(\boldsymbol{\beta}')|f'\rangle - \langle f'|\Gamma(\zeta')\otimes A(\boldsymbol{\beta}')|f'\rangle$ does not depend on the material phases κ_1, κ_{2o}, and κ_{2c}, nor on the laser phases $\text{Arg}\,\alpha_l$—provided that the phases of the local oscillator amplitudes $\boldsymbol{\beta}$ and $\boldsymbol{\beta}'$ are measured in reference to $\text{Arg}\,\alpha_l$, i.e.,

$$\beta_l = |\beta_l|\frac{\alpha_l}{|\alpha_l|}e^{\mathrm{i}\Delta_l}, \qquad \beta_l' = |\beta_l'|\frac{\alpha_l}{|\alpha_l|}e^{\mathrm{i}\Delta_l'}, \qquad \text{(D4)}$$

where $l = 1o, 2o, 1c, 2c$.

At this point, the following optimization variables can be identified: ζ, ζ', $|\beta_l|$, Δ_l, $|\beta_l'|$, and Δ_l'. Fixed parameters are ϕ, η, d_2, and the absolute laser amplitudes $|\alpha_l|$. According to the definitions (1) and (3) in the main text, the absolute amplitudes $|\alpha_l|$ are functions of certain empirical radial integrals D_1 and D_2, the values of which are not known at this point. In order to proceed with the optimization, we sample positive random values for

$$\frac{|\alpha_{1o}|}{\lambda}, \qquad \frac{|\alpha_{2o}|}{\sqrt{\lambda}}, \qquad \frac{|\alpha_{1c}|}{\lambda}, \qquad \frac{|\alpha_{2c}|}{\sqrt{\lambda}}, \qquad \text{(D5)}$$

and add the numerical scaling factor λ to the set of optimization variables. Globally optimal solutions have been acquired numerically by means of the covariance matrix adaptation evolution strategy (CMA-ES).[63] The numerical optimizations have been repeated for different samples of the absolute amplitudes. This has shown that the maximum violation of Ineq. (7) is independent of the particular random choice of the parameters (D5). The results are depicted in Fig. 3 in the main text. It is a plot of the maximally attainable value of $|\langle f'|B|f'\rangle|$ as a function of ϕ and for different detection efficiencies η.

The optimal values for λ, $|\beta_l|$, and $|\beta_l'|$, $l = 1o, 2o, 1c, 2c$, depend nontrivially on ϕ, η, and the parameters (D5). These values will therefore not be explicitly discussed. In contrast, the optimal values for ζ, ζ', Δ_l, and Δ_l' depend only on ϕ

and η and are piecewisely continuous in ϕ. Furthermore, the phases Δ_l, Δ'_l always fulfill

$$\Delta_{1o} = \Delta_{2o}, \qquad\qquad \Delta_{1c} = \Delta_{2c}, \qquad \text{(D6a)}$$

$$\Delta'_{1o} = \Delta'_{2o}, \qquad\qquad \Delta'_{1c} = \Delta'_{2c}. \qquad \text{(D6b)}$$

The case $d_2 \neq 0$ can be dealt with in a similar fashion as the case $d_2 = 0$ above. While we have not studied it systematically, we have verified numerically that, for several randomly chosen, non-perturbative complex values of d_2, the Bell-CHSH inequality can be violated to a substantial degree. Qualitatively, the effect of d_2 is to shift and distort the plot in Fig. 3, such that the maximum violation no longer occurs for $\phi = 0$.

[1] M. Shapiro and P. Brumer, *Quantum Control of Molecular Processes*, 2nd ed. (Wiley-VCH, Weinheim, 2012).

[2] S. Rice and M. Zhao, *Optical Control of Molecular Dynamics* (Wiley, 2000).

[3] M. Shapiro and P. Brumer, *Principles of the Quantum Control of Molecular Processes* (Wiley, New York, 2012).

[4] V. Constantoudis and C. A. Nicolaides, J. Chem. Phys. **122**, 084118 (2005).

[5] E. de Lima and M. de Aguiar, Phys. Rev. A **77**, 033406 (2008).

[6] M. Ivanov, D. Bartram, and O. Smirnova, Mol. Phys. **110**, 1801 (2012).

[7] M. Schlosshauer, *Decoherence and the Quantum-to-Classical Transition*, The Frontiers Collection (Springer, 2007).

[8] I. Franco and P. Brumer, Phys. Rev. Lett. **97**, 040402 (2006).

[9] I. Franco and P. Brumer, J. Phys. B **41**, 074003 (2008).

[10] L. A. Pachon and P. Brumer, J. Chem. Phys. **139**, 164123

[11] W. Miller, J. Chem. Phys. **136**, 210901 (2012).

[12] P. Brumer and M. Shapiro, Chem. Phys. Lett. **126**, 541 (1986).

[13] M. Shapiro, J. W. Hepburn, and P. Brumer, Chem. Phys. Lett. **149**, 451 (1988).

[14] J. S. Bell, Physics **1**, 195 (1964).

[15] J. Bell, Rev. Mod. Phys. **38**, 447 (1966).

[16] J. F. Clauser, M. A. Horne, A. Shimony, and R. A. Holt, Phys. Rev. Lett. **23**, 880 (1969).

[17] O. Gühne and G. Tóth, Phys. Rep. **474**, 1 (2009).

[18] R. Ionicioiu and D. R. Terno, Phys. Rev. Lett. **107**, 230406 (2011).

[19] A. Peruzzo, P. Shadbolt, N. Brunner, S. Popescu, and J. L. O'Brien, Science **338**, 634 (2012).

[20] F. Kaiser, T. Coudreau, P. Milman, D. B. Ostrowsky, and S. Tanzilli, Science **338**, 637 (2012).

[21] S. Flach, O. Yevtushenko, and Y. Zolotaryuk, Phys. Rev. Lett. **84**, 2358 (2000).

[22] L. Sirko and P. M. Koch, Phys. Rev. Lett. **89**, 274101 (2002).

[23] I. Franco, M. Spanner, and P. Brumer, Chem. Phys. **370**, 143 (2010).

[24] G. Greenstein and A. Zajonc, *The Quantum Challenge: Modern Research on the Foundations of Quantum Mechanics* (Jones and Bartlett, 2005).

[25] S. Haroche and J.-M. Raimond, *Exploring the Quantum: Atoms, Cavities and Photons* (Oxford University Press, Oxford, 2006).

[26] Y.-Y. Yin, C. Chen, D. S. Elliott, and A. V. Smith, Phys. Rev. Lett. **69**, 2353 (1992).

[27] Y.-Y. Yin and D. S. Elliott, Phys. Rev. A **47**, 2881 (1993).

[28] Z.-M. Wang and D. S. Elliott, Phys. Rev. Lett. **87**, 173001 (2001).

[29] Interference can of course still be observed with some weak recoil.

[30] U. Fano, Phys. Rev. **178**, 131 (1969).

[31] G. Baum, M. S. Lubell, and W. Raith, Phys. Rev. Lett. **25**, 267 (1970).

[32] J. R. Taylor, *Scattering Theory* (Wiley, 1972).

[33] H. Bethe and E. Salpeter, *Quantum Mechanics of One- and Two-Electron Atoms* (Dover, 2008).

[34] J. Gong and P. Brumer, J. Chem. Phys. **132**, 054306 (2010).

[35] C. Cohen-Tannoudji, J. Dupont-Roc, and G. Grynberg, *Atom-Photon Interactions: Basic Process and Applications* (Wiley, 1998).

[36] E. Fermi, Z. Phys. **59**, 680 (1930).

[37] M. J. Seaton, Proc. R. Soc., Ser. A **208**, 418 (1951).

[38] J. W. Cooper, Phys. Rev. **128**, 681 (1962).

[39] A. Burgess and M. J. Seaton, Mon. Not. R. Astron. Soc. **120**, 121 (1960).

[40] H. Bebb, Phys. Rev. **149**, 25 (1966).

[41] P. Lambropoulos and M. R. Teague, J. Phys. B **9**, 587 (1976).

[42] M. O. Scully, B.-G. Englert, and H. Walther, Nature (London) **351**, 111 (1991).

[43] W. M. Itano, J. C. Bergquist, J. J. Bollinger, D. J. Wineland, U. Eichmann, and M. G. Raizen, Phys. Rev. A **57**, 4176 (1998).

[44] B.-G. Englert, Acta Phys. Slov. **46**, 249 (1996).

[45] P. Bertet, S. Osnaghi, A. Rauschenbeutel, G. Nogues, A. Auffeves, M. Brune, J. M. Raimond, and S. Haroche, Nature (London) **411**, 166 (2001).

[46] N. Bohr, in *Quantum Theory and Measurement*, Princeton Series in Physics, edited by J. A. Wheeler, and W. H. Zurek (Princeton University Press, Princeton, NJ, 1983), Chap. I.1, pp. 9–49.

[47] B. Englert, Z. Naturforsch. **54a**, 11 (1998).

[48] J. A. Wheeler, in *Quantum Theory and Measurement*, Princeton Series in Physics, edited by J. A. Wheeler, and W. H. Zurek (Princeton University Press, Princeton, NJ, 1984), Chap. I.13, pp. 182–213.

[49] B. Sanders, Phys. Rev. A **45**, 6811 (1992).

[50] H. Jeong and N. B. An, Phys. Rev. A **74**, 022104 (2006).

[51] D. M. Greenberger, M. A. Horne, A. Shimony, and A. Zeilinger, Am. J. Phys. **58**, 1131 (1990).

[52] Specifically, entangled coherent states are produced from a single coherent light source (e.g., a laser) by letting the light interfere with itself in a MZI in which one arm has been replaced with a strong Kerr nonlinearity.[49] Furthermore, in order to prepare the initial state $|i\rangle$, it is not enough to create entangled light with a single frequency ω. This is because, compared to the two-photon ionization process, the one-photon process needs light with a doubled frequency 2ω. The next step in the preparation of $|i\rangle$ is therefore second harmonic generation which is also a nonlinear optical process. Further standard steps are used to balance the intensities of the beams and to adjust their phases and polarizations.

[53] J. Park, M. Saunders, Y. il Shin, K. An, and H. Jeong, Phys. Rev. A **85**, 022120 (2012).

[54] H. P. Yuen and J. Shapiro, IEEE Trans. Inf. Theory **26**, 78 (1980).

[55] J. Osterwalder, in *Magnetism: A Synchrotron Radiation Approach*, Lecture Notes in Physics Vol. 697, edited by E. Beaurepaire, H. Bulou, F. Scheurer, J.-P. Kappler, and J. Osterwalder (Springer, Berlin, 2006), pp. 95–120.

[56] B. S. Cirel'son, Lett. Math. Phys. **4**, 93 (1980).

[57] J. Barrett, N. Linden, S. Massar, S. Pironio, S. Popescu, and D. Roberts, Phys. Rev. A **71**, 022101 (2005).

[58] At the kinks of the ($\eta = 1$) graph, the global maximum switches between two different locally optimal solutions one of which is less robust to inefficient detection than the other. In case of the remaining graphs for which $\eta \leq 0.9$, the global optimum is provided by a variation of the more robust solution and kinks do thus not appear.

[59] J.-S. Tang, Y.-L. Li, X.-Y. Xu, G.-Y. Xiang, C.-F. Li, and G.-C. Guo, Nat. Photon. **6**, 602 (2012).

[60] S. S. Roy, A. Shukla, and T. S. Mahesh, Phys. Rev. A **85**, 022109 (2012).

[61] R. Auccaise, R. M. Serra, J. G. Filgueiras, R. S. Sarthour, I. S. Oliveira, and L. C. Céleri, Phys. Rev. A **85**, 032121 (2012).

[62] R. Stassi, A. Ridolfo, S. Savasta, R. Girlanda, and O. D. Stefano, EPL **99**, 24003 (2012).

[63] N. Hansen and A. Ostermeier, Evol. Comput. **9**, 159 (2001).

[64] R. Grimm, M. Weidemüller, and Y. B. Ovchinnikov, "Optical Dipole Traps for Neutral Atoms," in *Advances In Atomic, Molecular, and Optical Physics*, Vol. 42 (Academic Press, 2000), p. 95.

[65] J. Eschner, G. Morigi, F. Schmidt-Kaler, and R. Blatt, J. Opt. Soc. Am. B **20**, 1003 (2003).